The First Detection of a [C II] 158μm Emitter Associated with a Strong OI Absorber at the End of the Reionization Epoch

Yunjing Wu
Tsinghua University https://orcid.org/0000-0003-0111-8249
Zheng Cai (zcai@mail.tsinghua.edu.cn)
Tsinghua University
Marcel Neeleman
Max-Planck-Institut f¨ur Astronomie
Kristian Finlator
New Mexico State University https://orcid.org/0000-0002-0496-1656
Nissim Kanekar
National Cente for Radio Astrophysics https://orcid.org/0000-0002-9757-7206
Shiwu Zhang
Tsinghua University
Jason Prochaska
UCO/Lick Observatory https://orcid.org/0000-0002-7738-6875
Ran Wang
Kavli Institute for Astronomy and Astrophysics, Peking University
Xiaohui Fan
University of Arizona
Laura Keating
Leibniz-Institut für Astrophysik Potsdam https://orcid.org/0000-0001-5211-1958
Feige Wang
Steward Observatory, University of Arizona
Jinyi Yang
Steward Observatory, University of Arizona
Joseph Hennawi
University of California Santa Barbara https://orcid.org/0000-0002-7054-4332
Junxian Wang
University of Science and Technology of China https://orcid.org/0000-0002-4419-6434

Letter

Keywords: [C II] 158μm emission, OI absorber, reionization epoch

Posted Date: December 15th, 2020

DOI: https://doi.org/10.21203/rs.3.rs-124668/v1

Version of Record: A version of this preprint was published at Nature Astronomy on September 27th, 2021. See the published version at https://doi.org/10.1038/s41550-021-01471-4.

The First Detection of a [C II] 158μm Emitter Associated with a Strong OI Absorber at the End of the Reionization Epoch

Yunjing Wu[1], Zheng Cai[1*], Marcel Neeleman[2], Kristian Finlator[3], Nissim Kanekar[4], Shiwu Zhang[1], J. Xavier Prochaska[5,6], Ran Wang[7], Xiaohui Fan[8], Laura C. Keating[9], Feige Wang[8,13], Jinyi Yang[8,14], Joseph F. Hennawi[10], Junxian Wang[11,12]

[1]*Department of Astronomy, Tsinghua University, Beijing 100084, China*

[2]*Max-Planck-Institut für Astronomie, Königstuhl 17, D-69117, Heidelberg, Germany*

[3]*New Mexico State University, Las Cruces, 88003 NM, USA*

[4]*National Centre for Radio Astrophysics, Tata Institute of Fundamental Research, Pune University, Pune 411007, India*

[5]*Department of Astronomy & Astrophysics, UCO/Lick Observatory, University of California, 1156 High Street, Santa Cruz, CA 95064, USA*

[6]*Kavli Institute for the Physics and Mathematics of the Universe (Kavli IPMU), The University of Tokyo, 5-1-5 Kashiwanoha, Kashiwa, 277-8583, Japan*

[7]*Kavli Institute for Astronomy and Astrophysics, Peking University, Beijing 100871, China*

[8]*Steward Observatory, University of Arizona, 933 North Cherry Avenue, Tucson, AZ 85721, USA*

[9]*Canadian Institute for Theoretical Astrophysics, University of Toronto, 60 St. George Street, Toronto, ON M5S 3H8, Canada*

[10]*Department of Physics, University of California, Santa Barbara, CA 93106-9530, USA*

[11]*CAS Key Laboratory for Research in Galaxies and Cosmology, Department of Astronomy, Uni-*

versity of Science and Technology of China, Hefei, Anhui 230026, China

[12] *School of Astronomy and Space Science, University of Science and Technology of China, Hefei 230026, China*

[13] *Hubble Fellow*

[14] *Strittmatter Fellow*

The physical and chemical properties of the circumgalactic medium (CGM) at $z \gtrsim 6$ have been studied successfully through the absorption in the spectra of background Quasi-Stellar Objects (QSOs) [1–3]. One of the most crucial questions is to investigate the nature and location of the source galaxies that give rise to these early metal absorbers[4–6]. Theoretical models suggest that momentum-driven outflows from typical star-forming galaxies can eject metals into the CGM and the intergalactic medium (IGM), with the projected separation between absorbers and galaxies expected to range from 5 to 50 proper kpc at z=5–6 [7–10]. Deep, dedicated surveys have searched for Lyα emission associated with strong CIV absorbers at $z \approx 6$, but only a few Lyα emitter candidates have been detected. Interpreting these detections is moreover ambiguous because Lyα is a resonant line[11–13], raising the need for complementary techniques for detecting absorbers' host galaxies. Here, using Atacama Large Millimeter Array (ALMA), we report, for the first time, the [C II] 158μm emission and the far-infrared dust continuum associated with a strong low-ionization absorber, O I, at $z = 5.978$. The [C II] luminosity is 73 million solar luminosities, corresponding to a dark matter halo mass of 100 billion solar masses. This is one to two orders of magnitude more massive than typical values predicted from cosmological simulations[9,16].

Metal absorption systems (e.g., O I, C IV, and Mg II) are powerful probes of the enrichment of the high-redshift intergalactic medium (IGM) [1–3]. Because the first excitation energies of O I and neutral hydrogen are almost identical, O I is considered one of the best indicators to trace the metal enrichment and the neutral IGM close to the reionization epoch[14,15]. Cosmological simulations suggest that at $z = 5 - 6$, feedback from typical star-forming galaxies can eject metals such as oxygen up to 50 proper kpc, corresponding to projected separations of $\approx 9''$ [8–10]. Thus, measurements of the impact parameters and the star formation rates (SFRs) of the source galaxies can strongly constrain the efficiency of galactic winds in transporting metals and then test different feedback models [16]. Here we show our ALMA band-6 observations centered on one of the strongest O I absorber at $z = 5.978$ toward QSO J2054−0005. The absorber has a rest-frame equivalent width (REW) of 0.12Å [17], corresponding to the best-fit column density of $10^{14.2}$ cm^{-2} in the small optical depths regime (ref.[16]). The source galaxy we detected has a [C II] luminosity of 73 million solar luminosities, one to two orders of magnitude brighter than typical luminosities predicted by cosmological simulations[9,16,18–20].

The [C II] pseudo-narrow band image shown in Fig. 1a is constructed by collapsing the emission line channels from the [C II] data cube. At the redshift of the O I absorber, an emission line is detected at 6-σ significance which we interpret as [C II] emission from a galaxy at the O I absorber's redshift. We refer this [C II] emitter as [C II]2054 in the following. We show the spectrum of [C II]2054 in the bottom-right panel of Fig. 1. The yellow shaded region represents the collapsed channels. The velocity-integrated [C II] flux density is measured to be 0.078 ± 0.013 Jy km s^{-1}. From the pseudo-narrow band image, the projected impact parameter between [C II]2054 and the

O I absorber is 3.5″ , corresponding to 20.0 proper kpc (pkpc) at $z = 5.978$. Throughout this paper we use $\Omega_\Lambda = 0.7$, $\Omega_\mathrm{M} = 0.3$ and $H_0 = 70$ km s^{-1} Mpc^{-1}.

Other than QSO J2054, in the far-infrared dust-continuum image (Fig. 1b), we detect another five continuum targets with signal-to-noise ratio above five. The archival Hubble Space Telescope (*HST*) broad-band data have been used to estimate their photometric redshifts [21]. All of these galaxies are securely identified as foreground sources which do not associate with the O I absorber at $z = 6$ (color selection shown in Methods).

The [C II] 158-μm fine structure line emission is the dominant cooling line in the interstellar medium, and it is almost unaffected by dust attenuation[22,23]. ALMA allows us to use [C II] to probe the physical conditions of the gas in galaxies, and quantify the star formation rate (SFR) of the galaxy in the post-reionzation epoch[24]. The velocity-integrated [C II] luminosity of [C II]2054 is estimated to $L_{[\mathrm{CII}]} = (7.3 \pm 1.2) \times 10^7 L_\odot$ [25], corresponding to a [C II]-based SFR ($\mathrm{SFR}_{[\mathrm{CII}]}$) of $\approx 5.7 \pm 1.1 M_\odot$ yr^{-1} (ref. [26]). No submillimeter continuum is detected at the position of [C II]2054, yielding a 3-σ upper limit of 39 μJy. Converting this luminosity to a total infrared SFR ($\mathrm{SFR}_\mathrm{TIR}$) yields the upper limit $\mathrm{SFR}_\mathrm{TIR} < 5.2\ M_\odot$ yr^{-1} (ref. [27]). The derived stellar mass of [C II]2054 is estimated to be $4.2 \times 10^8 M_\odot$, and the halo mass is estimated to be $9.1 \times 10^{10}\ M_\odot$ (with 0.3 dex systematic uncertainty in both of the conversions)[29] (see Methods).

To constrain models of IGM metal enrichment at the end of reionization, we compare our observed impact parameter against predictions from the Illustris, Sherwood, HVEL, and FAST cosmological hydrodynamic simulations[16,18–20]. As mentioned above, the O I absorber has a REW of

0.12Å, and the measured projected impact parameter is 20.0 pkpc (Fig. 1c). Broadly, simulations predict that metal line absorbers with REW of 0.12 ± 0.05 Å arise at impact parameters of 5–30 pkpc, bracketing our measurement. Specifically, in Fig. 2 (left panel), we show the comparison of our data with the Illustris simulation[16]. The comparisons with other simulations are also shown in extended Fig. 3 in Methods. In this panel, the red star shows our observations, while other points are from the Illustris simulation. The simulation is able to predict our observed impact parameter, and has demonstrated that galaxies similar to [C II]2054 are able to enrich the IGM at distances of $\gtrsim 20$ pkpc. Nevertheless, one should also note that 11.1% of the data points in the simulation have a similar or larger impact parameter than that of [C II]2054. Thus, the O I absorber associated with [C II]2054 arises at a somewhat larger distance from its host galaxy than that would be expected from hydrodynamical simulations.

Other than the projected impact parameter, different simulations also have clear predictions of the SFR, stellar mass, or halo mass of the source galaxies. For a direct comparison of the models, we need to derive the stellar or halo mass of [C II]2054 based on SFR. As we mentioned above, [C II]2054 has a stellar mass of $4.2 \times 10^8\ M_\odot$ and a halo mass of $9.1 \times 10^{10}\ M_\odot$. Different simulations, including Illustris, Sherwood, HVEL, and FAST simulations, directly investigated the halo mass distribution for O I absorbers with column densities of $N_{\rm OI} > 10^{14}\ {\rm cm}^{-2}$ at $z = 6$. They find that O I absorbers with REW in the range 0.12 ± 0.05 Å at $z = 6$ are typically embedded in $10^{9-10}\ {\rm M}_\odot$ halos [9,16]. This value is one to two orders of magnitude smaller than that implied by our observations. Thus our results suggest that low-mass systems in these simulations are likely to be overly efficient at producing metal absorbers.

A caveat to this result stems from the fact that the analysis of these simulations identified each metal absorber with its nearest halo. In reality, the nearest halo may not necessarily to be the true source of an absorber because a halo that is slightly more distant but significantly more massive may contribute more of its metals. This consideration indicates the need for an alternative framework for quantifying the galaxy-absorber relationship that can circumvent this ambiguity.

Recently, a set of Technicolor Dawn simulations have been developed, aiming to enable a detailed study of the metal enrichment of galaxies in the reionization epoch [10]. This set of simulations incorporates realistic small-scale UV background fluctuations and reproduces a broad range of observations of reionization and early galaxy growth [10]. They simultaneously reproduce observations of the galaxy stellar mass function, the Si IV column density distribution, and the UVB amplitude at $z > 5$. Hence, the galaxy populations and their metallicity of the circumgalactic medium (CGM) are realistic.

Our discovery of [C II]2054 is not expected from the Technicolor Dawn simulations. In Fig. 2 (right panel), we show how the number of galaxies that cluster about strong O I absorbers at $z = 6$ is predicted to vary with [C II]-based SFR. The solid and dashed curves are generated by compiling catalogs of all galaxies that fall within 50 or 100 pkpc from strong O I absorbers, respectively. The strong O I absorbers have rest-frame equivalent widths of REW > 0.12Å ($N_{\rm OI} > 10^{14.2}{\rm cm}^{-2}$). The SFR on the lower x-axis is the 100-Myr average for physically-associated galaxies, while the top x-axis converts this SFR to $L_{\rm [CII]}$[26]. We plot [C II]2054's SFR in this panel using red square with error bar. Consistent with previous simulations [8,9], Technicolor Dawn simulations predict that the

characteristic luminosity of physically-associated [C II] emitters should be roughly two orders of magnitude lower in $L_{[\mathrm{CII}]}$ than [C II]2054; that is, far fewer than one such galaxy is predicted to lie within the area probed by our ALMA observation.

While Fig. 2 suggests that our observation is largely unexpected, we note that the cosmological volume of Technicolor Dawn simulations remains relatively small to contain a representative population of bright galaxies ($M_{\mathrm{UV}} < -20$)[10]. Nonetheless, a fair quantitative comparison can still be conducted. We further quantify the discrepency between simulations and observations by re-casting the observations as a constraint on the galaxy-absorber cross-correlation function. Based on the [C II] luminosity function at this redshift [30], the mean space density of galaxies at $z = 5.9$ with the SFR$\geq 5.7 M_{\odot}$ yr^{-1} is 0.0144 cMpc^{-3}. A sphere of radius 20 pkpc containing one such galaxy has a mean overdensity of $\Delta = 6.042 \times 10^3$. Our observations therefore confirm that bright galaxies and strong absorbers correlate strongly [6,10]. We quantify this correlation using the galaxy-absorber cross-correlation function $\xi(r) = (r/r_0)^{-\gamma}$, which expresses the fractional excess number density of galaxies located at a distance r from an absorber in terms of the correlation length r_0 and a power-law slope γ.

In Fig. 3, we use solid red curves to show combinations of r_0 and γ that predict an average of one galaxy within 20.0 pkpc of an absorber at $z = 5.9$. Shaped points indicate cross-correlation functions directly predicted by Technicolor Dawn for galaxies clustered about synthetic OI absorbers with REW ≥ 0.12Å. As galaxies with SFR$\geq 5.7 M_{\odot}$ yr^{-1} are too rare to arise in the current simulation volume, we consider three lower SFR thresholds (see the legend). In all cases,

the predicted r_0 is $\sim 10\times$ too low to explain the observation. Moreover, while r_0 does increase with SFR threshold [10], the trend is not nearly strong enough to explain the discrepancy.

[C II]2054 may be explained if its SFR were overestimated because faint galaxies are more abundant than bright ones. For example, it could be undergoing a temporary starburst. Alternatively, a strong intervening gravitational lens could boost its flux. To evaluate whether these possibilities would be sufficient to explain our observations, we use dashed and dotted curves to plot combinations of r_0 and γ that would explain [C II]2054 if its true SFR were ten and 100 times lower, respectively. Even in these cases, the simulation underpredicts r_0 by a factor of 10.

In summary, our first ALMA detection of a [C II] emitter associated with a reionization-epoch O I absorber is more than one to two orders of magnitude higher in [C II] luminosity than expected from hydrodynamical simulations. Casting this observation as a constraint on the galaxy-absorber cross-correlation function suggests that the correlation length predicted by Technicolor Dawn is $\sim 10\times$ too low. These observations could indicate that low-mass galaxies are too efficient at creating and/or expelling metals in hydrodynamical simulations, or that our ALMA observations lead us to overestimate the underlying SFR of [C II]2054. Future surveys will be needed to test conclusively whether bright galaxies are more common about strong O I absorbers than expected from current theoretical models, as currently suggested by our data. Meanwhile, testing the strong prediction that many faint galaxies should exist in the vicinity of our O I absorber will require a much deeper survey using the *James Weber Space Telescope (JWST)*.

1. Codoreanu, A. *et al.* The comoving mass density of Mg II from z $\sim$ 2 to 5.5. *MNRAS* **472**, 1023–1051 (2017). 1708.00304.

2. Becker, G. D. *et al.* The Evolution of O I over 3.2 < z < 6.5: Reionization of the Circumgalactic Medium. *APJ* **883**, 163 (2019). 1907.02983.

3. Cooper, T. J. *et al.* Heavy Element Absorption Systems at 5.0 < z < 6.8: Metal-poor Neutral Gas and a Diminishing Signature of Highly Ionized Circumgalactic Matter. *APJ* **882**, 77 (2019). 1901.05980.

4. Cai, Z., Fan, X., Dave, R., Finlator, K. & Oppenheimer, B. Probing the Metal Enrichment of the Intergalactic Medium at z = 5-6 Using the Hubble Space Telescope. *APJL* **849**, L18 (2017). 1709.10111.

5. Bielby, R. M. *et al.* Into the Ly α jungle: exploring the circumgalactic medium of galaxies at z $\sim$ 4-5 with MUSE. *MNRAS* **493**, 5336–5356 (2020). 2001.09058.

6. Díaz, C. G. *et al.* Faint LAEs near z>4.7 CIV absorbers revealed by MUSE. *arXiv e-prints* arXiv:2001.04453 (2020). 2001.04453.

7. Oppenheimer, B. D. & Davé, R. Cosmological simulations of intergalactic medium enrichment from galactic outflows. *MNRAS* **373**, 1265–1292 (2006). astro-ph/0605651.

8. Oppenheimer, B. D., Davé, R. & Finlator, K. Tracing the re-ionization-epoch intergalactic medium with metal absorption lines. *MNRAS* **396**, 729–758 (2009). 0901.0286.

9. Finlator, K. *et al.* The host haloes of O I absorbers in the reionization epoch. *MNRAS* **436**, 1818–1835 (2013). 1305.4768.

10. Finlator, K., Doughty, C., Cai, Z. & Díaz, G. The faint host galaxies of C IV absorbers at z > 5. *MNRAS* **493**, 3223–3237 (2020). 2001.03498.

11. Dijkstra, M., Haiman, Z. & Spaans, M. Lyα Radiation from Collapsing Protogalaxies. I. Characteristics of the Emergent Spectrum. *APJ* **649**, 14–36 (2006). astro-ph/0510407.

12. Zheng, Z., Cen, R., Trac, H. & Miralda-Escudé, J. Radiative Transfer Modeling of Lyα Emitters. I. Statistics of Spectra and Luminosity. *APJ* **716**, 574–598 (2010). 0910.2712.

13. Hayes, M. *et al.* Escape of about five per cent of Lyman-α photons from high-redshift star-forming galaxies. *Nature* **464**, 562–565 (2010). 1002.4876.

14. Oh, S. P. Probing the dark ages with metal absorption lines. *MNRAS* **336**, 1021–1029 (2002). astro-ph/0201517.

15. Furlanetto, S. R. & Loeb, A. Metal Absorption Lines as Probes of the Intergalactic Medium Prior to the Reionization Epoch. *APJ* **588**, 18–34 (2003). astro-ph/0211496.

16. Keating, L. C., Puchwein, E., Haehnelt, M. G., Bird, S. & Bolton, J. S. Testing the effect of galactic feedback on the IGM at z $\sim$ 6 with metal-line absorbers. *MNRAS* **461**, 606–626 (2016). 1603.03332.

17. Becker, G. D., Sargent, W. L. W., Rauch, M. & Calverley, A. P. High-redshift Metals. II. Probing Reionization Galaxies with Low-ionization Absorption Lines at Redshift Six. *APJ* **735**, 93 (2011). 1101.4399.

18. Vogelsberger, M. *et al.* Properties of galaxies reproduced by a hydrodynamic simulation. *NAT* **509**, 177–182 (2014). 1405.1418.

19. Bolton, J. S. *et al.* The Sherwood simulation suite: overview and data comparisons with the Lyman α forest at redshifts $2 \leq z \leq 5$. *MNRAS* **464**, 897–914 (2017). 1605.03462.

20. Bird, S. *et al.* Damped Lyman α absorbers as a probe of stellar feedback. *MNRAS* **445**, 2313–2324 (2014). 1405.3994.

21. Mechtley, M. *et al.* Do the Most Massive Black Holes at z = 2 Grow via Major Mergers? *APJ* **830**, 156 (2016). 1510.08461.

22. De Looze, I., Baes, M., Bendo, G. J., Cortese, L. & Fritz, J. The reliability of [C II] as an indicator of the star formation rate. *MNRAS* **416**, 2712–2724 (2011). 1106.1643.

23. Carilli, C. L. & Walter, F. Cool Gas in High-Redshift Galaxies. *ARAA* **51**, 105–161 (2013). 1301.0371.

24. Lagache, G., Cousin, M. & Chatzikos, M. The [CII] 158 μm line emission in high-redshift galaxies. *AAP* **609**, A130 (2018). 1711.00798.

25. Wang, R. *et al.* Star Formation and Gas Kinematics of Quasar Host Galaxies at z ~6: New Insights from ALMA. *APJ* **773**, 44 (2013). 1302.4154.

26. De Looze, I. *et al.* The applicability of far-infrared fine-structure lines as star formation rate tracers over wide ranges of metallicities and galaxy types. *AAP* **568**, A62 (2014). 1402.4075.

27. Izumi, T. *et al.* Subaru High-z Exploration of Low-Luminosity Quasars (SHELLQs). III. Star formation properties of the host galaxies at z $\gtrsim$ 6 studied with ALMA. *PASJ* **70**, 36 (2018). 1802.05742.

28. Salmon, B. *et al.* The Relation between Star Formation Rate and Stellar Mass for Galaxies at 3.5 $\leq$ z $\leq$ 6.5 in CANDELS. *APJ* **799**, 183 (2015). 1407.6012.

29. Ma, X. *et al.* Simulating galaxies in the reionization era with FIRE-2: galaxy scaling relations, stellar mass functions, and luminosity functions. *MNRAS* **478**, 1694–1715 (2018). 1706.06605.

30. Yan, L. *et al.* The ALPINE-ALMA [C II] Survey: [C II]158micron Emission Line Luminosity Functions at $z \sim 4-6$. *arXiv e-prints* arXiv:2006.04835 (2020). 2006.04835.

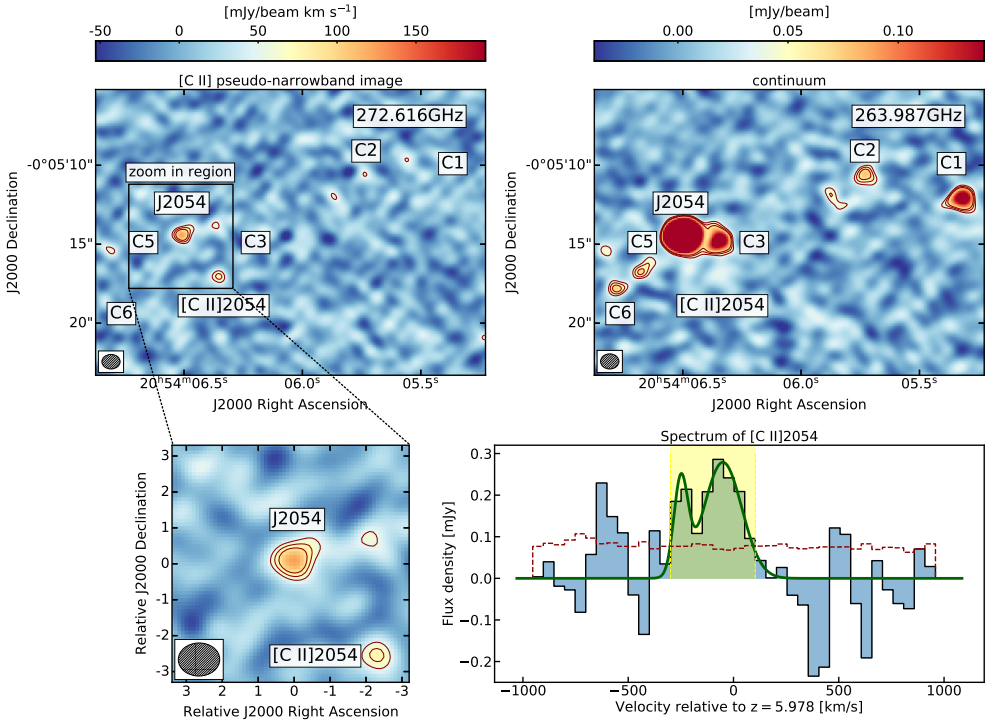

Fig. 1. ALMA observations. a, Integrated [C II] pseudo-narrowband image. The outer contour is at 3σ level, with contours in steps of 1-σ. The 1-σ is 1.76×10^{-2}Jy beam^{-1} km s^{-1}, calculated using the pixel-to-pixel standard deviation. The QSO is detected in the continuum-subtracted image because of a water line at this frequency. **b,** 263.987 GHz continuum map. Contours are drawn at $[3, 4, 5] \times \sigma$. In this map, the 1-σ noise is 12.6 μJy beam^{-1}. Six continuum sources within 20″ can be seen. C4 is the QSO J2054. **c,** Zoom-in [C II] pseudo-narrow band image. The sizes of the synthesized beams are plotted in the bottom-left of these panel. **d,** Spectrum of [C II]2054. The darked dashed line shows the 1-σ rms noise. The narrow-band [C II] image is collapsed based on the emission range shown by the yellow-shaded region. The velocity is relative to the O I redshift $z = 5.978$. The darkgreen line shows a double Gaussian model fit to the data. The integral [C II] flux is 0.078 ± 0.013 Jy km s^{-1}.

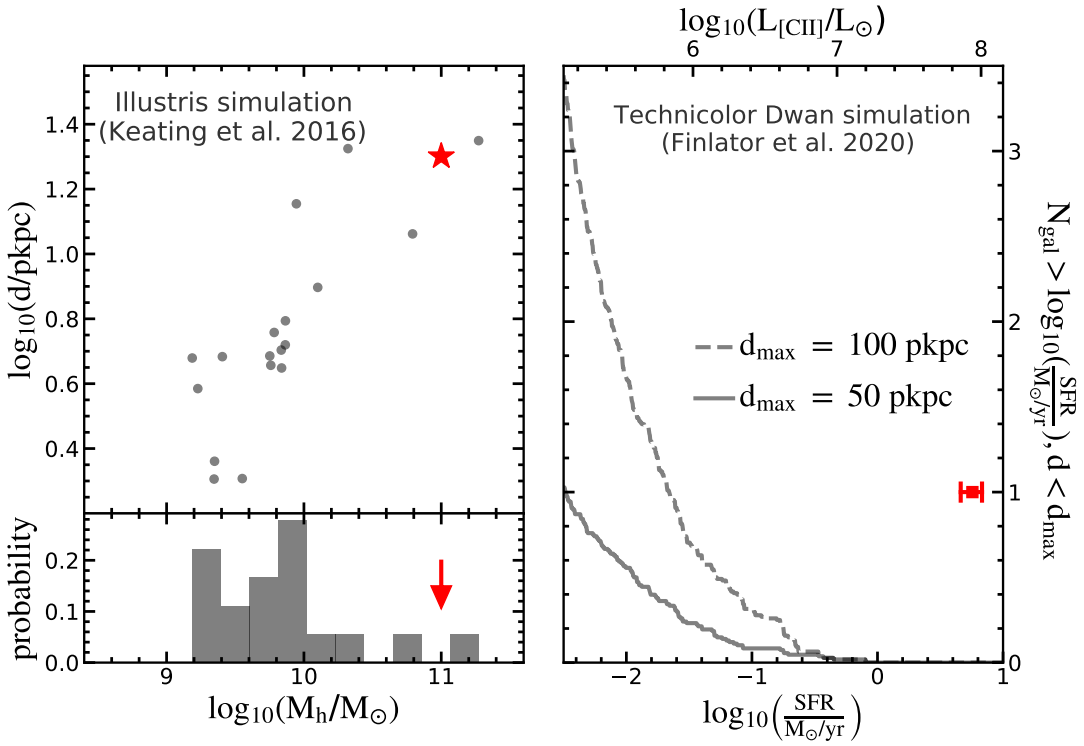

Fig. 2. Comparison between simulations and observations. Left Upper: The relationship between projected impact parameter and halo mass of strong O I absorbers in the Illustris simulation[16]. The O I absorbers have the rest-frame equivalent width of 0.12 ± 0.05 Å (consistent with observations). Red star represents [C II]2054. **Left Bottom:** Red arrow shows that the host halo mass of [C II]2054 is larger than one order of magnitude than the median value predicted by Illustris simulations. **Right:** The number of galaxies that cluster about strong O I absorbers at $z = 6$ is predicted to vary with SFR (y-axis is arbitrary). The solid and dashed curves are biased star formation rate functions [10]. They are generated by accumulating catalogs of all galaxies that fall within 50 or 100 pkpc of O I absorbers with REW > 0.12Å ($N_{\rm O\,I} > 10^{14.2}{\rm cm}^{-2}$). The predicted luminosity of O I associated [C II] emitter is roughly two orders of magnitude fainter than [C II]2054.

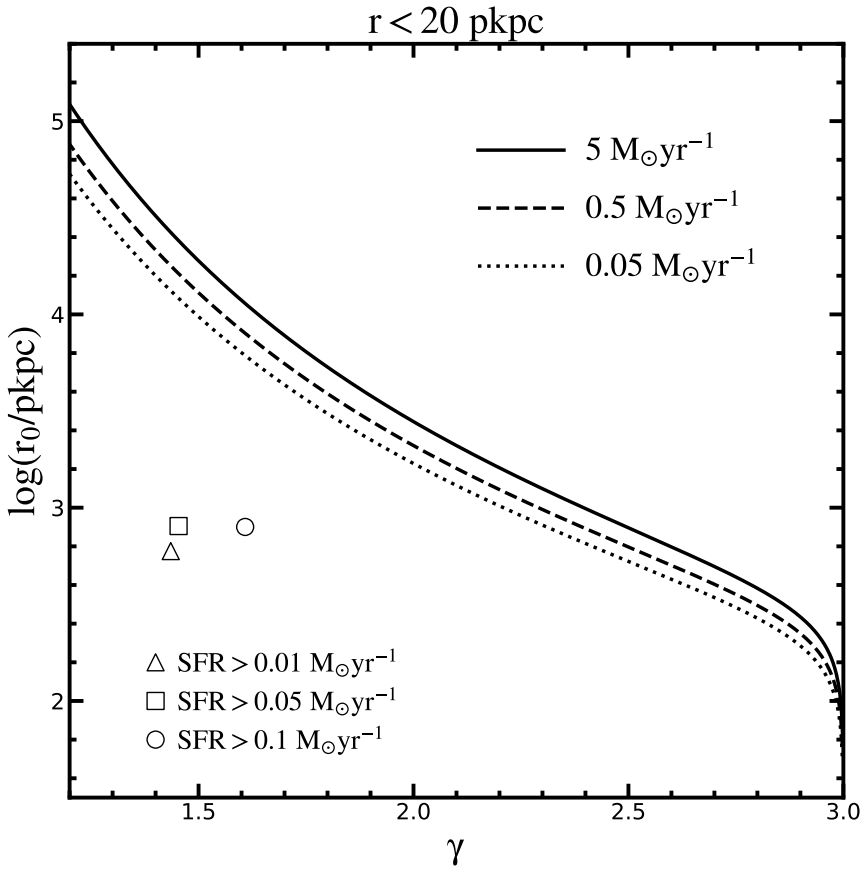

Fig. 3. Comparison of cross-correlation function between simulations and observations. We assume the galaxy-absorber cross-correlation as $\xi(r) = (r/r_0)^{-\gamma}$. This function expresses the fractional excess number density of galaxies located at a distance r from an absorber in terms of the correlation length r_0 and a power-law slope γ. Shaped points indicate cross-correlation functions predicted by Technicolor Dawn for galaxies clustered about synthetic OI absorbers with REW ≥ 0.12Å. The solid, dashed and dotted line shows that predict an average of one galaxy of SFR $\geq 5,\ 0.5$ and $0.05\ \mathrm{M}_\odot/\mathrm{yr}$, within 20.0 pkpc of an absorber at $z = 5.9$, respectively. Comparing with shaped dots, the predicted r_0 is $\sim 10\times$ too low to explain the observations.

ALMA continuum image					
Source name	S_{264}[a] (mJy)		$flux_{\rm err}$ (mJy)		S/N
C1	0.25		0.03		8
C2	0.15		0.05		5
C3	0.31		0.05		6
J2054	3.34		0.04		84
C5	0.13		0.025		5
C6	0.08		0.01		6
[C II] pseudo-narrowband map					
Source name	$flux_{\rm [C\,II]}$ (Jy kms^{-1})		$flux_{\rm err}$ (Jy kms^{-1})		S/N
[C II]2054	0.078		0.013		6
HST observations					
Source name[b]	F606W(V)	F814W(I)	F105W(Y)	F125W(J)	F160W(H)
C1-1	28.95 ± 0.54	27.74 ± 0.28	27.48 ± 0.11	27.09 ± 0.04	26.61 ± 0.03
C1-2	28.43 ± 0.34	27.30 ± 0.19	26.42 ± 0.04	25.92 ± 0.01	25.57 ± 0.01
C1-3	27.91 ± 0.21	27.54 ± 0.23	26.47 ± 0.04	25.80 ± 0.01	25.35 ± 0.01
C2	−[c]	−[c]	25.98 ± 0.03	25.62 ± 0.01	25.21 ± 0.01
C3-1	28.13 ± 0.25	27.40 ± 0.20	26.65 ± 0.05	26.30 ± 0.02	26.04 ± 0.02
C3-2	25.15 ± 0.02	24.63 ± 0.02	24.44 ± 0.01	24.421 ± 0.004	24.275 ± 0.004
C3-3	28.22 ± 0.28	27.39 ± 0.20	26.69 ± 0.05	26.31 ± 0.02	26.00 ± 0.02
J2054	26.75 ± 0.07	22.255 ± 0.002	21.517 ± 0.001	21.441 ± 0.001	21.248 ± 0.001
C5-1	27.53 ± 0.15	26.92 ± 0.13	26.63 ± 0.05	26.66 ± 0.03	26.49 ± 0.03
C5-2	28.26 ± 0.29	27.00 ± 0.14	26.67 ± 0.05	26.69 ± 0.03	26.65 ± 0.03
C5-3	28.95 ± 0.54	28.33 ± 0.48	27.69 ± 0.13	27.51 ± 0.06	26.92 ± 0.04
C6	27.27 ± 0.12	26.48 ± 0.09	25.30 ± 0.01	24.83 ± 0.01	24.48 ± 0.01

[a] Continuum flux density at 264 GHz
[b] *HST* resolves these sources as multi targets. We number the resolved sources from 1 to 3.
[c] C2 is located in the gap of two CCD chips. Therefore, C2 does not have these magnitudes.

Table 1. Photometric Results of sources in J2054 field. In our ALMA observations, for each source, 2-σ contour areas are regarded as emission regions. We use these emission regions as the photometric aperture for resolved sources, while for unresolved sources, the peak surface brightness represents the total flux. For HST observations, we used a uniform aperture with 0.3″ diameter.

Methods

Cosmology. In this paper, we assume a flat cosmological model with $\Omega_{\rm M} = 0.3, \Omega_{\lambda} = 0.7$ and $\rm H_0 = 70\,km\,s^{-1}\,Mpc^{-1}$. In this cosmology, at $z = 5.978$, $1''$ corresponds to approximately 5.7 kpc.

ALMA observations and data reduction. There are a few advantages of using ALMA to probe the source galaxies associated with OI absorber at $z \approx 6$. Firstly, the sub-mm [C II] 158μm line is one of the strongest far-infrared lines from galaxies [22,23]. Secondly, the background QSO is less dominant in emission at sub-millimeter regime. Thirdly, at this redshift, [C II] emission is shifted within ALMA band-6, which has a high throughput and is thus efficient for emission line detections. Finally, cosmological simulations suggest that O I absorbers have a relatively small halo, with predicted impact parameters less than $10''$, perfectly within the ALMA field of view[16].

The ALMA observations used four 1.875 GHz spectral windows (SPWs). Each SPW was divided into 43 channels. Two of the SPWs were centered on the [C II] emission at the redshift of O I absorber and QSO respectively. The remaining two SPWs were used to obtain a continuum image of the field. The on-source time was 2.8 hours. Data were reduced with the ALMA pipeline, which is part of the Common Astronomy Software Application (CASA)[28]. The flux scale was calibrated by observing J2148+0657, whereas the phase stability was checked by observing J2101+0341. Absolute flux uncertainties are expected to be less than 10%.

The final data cubes and continuum images were obtained using natural weighting in order to maximize sensitivity. This resulted in a beam size of $1.2'' \times 1.0\,''$ and a 1-σ background standard

deviation of 12.6 μJy beam^{-1} for the continuum image. A pseudo-narrow band image was also generated centered on the redshifted [C II] emission line. For the pseudo-narrow band image, the emission line channels were collapsed resulting in a beam size of $1.2'' \times 0.9''$ and a 1-σ sensitivity of 1.764×10^{-2}Jy beam^{-1} km s^{-1}. For each source, 2-σ contour areas are regarded as emission regions. We use these emission regions as the photometric aperture for resolved sources, while for unresolved sources, the peak surface brightness represents the total flux. The photometry results are shown in Table 1.

HST Broadband Imaging. For the field surrounding QSO J2054−0005, the *HST* archival database has two optical observations F606W(V) and F814W(I) [21] and three near-infrared broadband images F105W(Y), F125W(J) and F160W(H) (PID: 15064, PI: Caitlin Casey). These broad filter images are used to estimate the photometric redshifts of targets in this field through the use of the Lyman break drop-out technique [29]. Galaxies at $z \approx 6$ are expected to drop out of the F606W filter. We have remeasured the photometry of the galaxies using SExtractor [30] with a uniform $0.3''$ diameter aperture. Table 1 shows the HST-broadband photometric results of all the ALMA-detected continuum sources. Extended Data Fig. 1 shows the five broadband observations.

[C II] luminosity, SFR and halo mass estimation The velocity-integrated [C II] flux density is measured to be 0.078 ± 0.013 Jy km s^{-1}, corresponding to a luminosity of $L_{\rm [C\,II]} = (7.3 \pm 1.2) \times 10^7 L_\odot$. $L_{\rm [C\,II]}/L_\odot = 1.04 \times 10^{-3} S\Delta v \nu_0 (1+z)^{-1} D_L^2$ [25], $\nu_0 = 1900.5369$GHz is the rest frame [C II] line frequency, $S\Delta v$ is the integrated line flux in Jy km s^{-1}, and D_L is the luminosity distance in Mpc. [C II]-based SFR, $\rm SFR_{[CII]} \approx 5.7 \pm 1.1 M_\odot\ yr^{-1}$ ($\log \rm SFR = -8.52 + 1.18 \times \log L_{[C\,II]}$[26]). To obtain the estimated halo mass, firstly, we estimate the $\rm SFR_{[C\,II]}$ using Equation 17 of ref. [26]

(with 0.3 dex uncertainty). Moreover, we assume that the [C II]- and UV-based SFR are consistent with each other to derive the stellar mass based on $\mathrm{SFR}_{\mathrm{[C\,II]}}$. Using the empirical relation of ref.[28], the predicted stellar mass of [C II]2054 is $4.2 \times 10^8\ M_\odot$, with 0.3 dex uncertainty. Further, we estimate the halo mass of this absorber based on Equation 1 of ref.[29]. The predicted halo mass is about $9.1 \times 10^{10} M_\odot$ (with 0.3 dex uncertainty).

[C II]2054 continuum properties. No continuum was detected at the position of [C II]2054, resulting in a 3-σ upper limit of 39 μJy beam^{-1}. To convert this continuum flux to a total infrared luminosity (TIR; 8-1000μm), we estimate the TIR luminosity by fitting a modified blackbody (i.e., $S_\nu \sim \nu^\beta/(\exp(\mathrm{h}\nu/\mathrm{kT_{dust}}) - 1)$) to this single upper limit. We assume [C II]2054 has the same continuum properties as a typical Lyman break galaxy at this redshift, therefore we adopt a dust temperature of $T_{\mathrm{dust}} = 33$K and emissivity index of $\beta = 1.6$ [31]. This results in a 3-σ upper limit of L_{TIR} of $3.5 \times 10^{10}\ L_\odot$. Converting this luminosity to a SFR estimate, $\mathrm{SFR_{TIR}}$, yields $\mathrm{SFR_{TIR}} < 5.2\ M_\odot\ \mathrm{yr}^{-1}$ [27].

[C II]2054 also was not detected in any of the HST broadband imaging (Extended Data Fig. 1). From the HST imaging, we determine a 3-σ upper limit of the UV continuum at the position of [C II]2054 of 3.413×10^{44} erg s^{-1} (F105W band). This corresponding to an upper limit of the UV-based SFR of $\mathrm{SFR_{UV}} < 15\ M_\odot\ \mathrm{yr}^{-1}$.

Continuum sources. There are five *HST* broad-band observations in this field (F606W(V), F814W(I), F105W(Y), F125W(J), F160W(H)), the photometric results for each source are tabulated in Table 1. To constrain the photometric redshifts of these continuum sources, we use color-color

diagrams as shown in Extended Data Fig. 2, and compare the colors of the galaxies with those colors of simulated galaxies. In the *HST* image (Extended Data Fig. 1), C1, C3, C5 are resolved as multiple targets. Therefore, we plot the colors of these multiple sources individually.

For the model galaxies, we use a general star-forming galaxies approach [32]. Model spectra of different galaxies at different redshifts are generated from the models presented in BC03 [33]. For the galaxy models, we take the metallicity to be $Z = 0.02Z_{\odot}$, with an age of 25 Myr, and we assume a Salpeter initial mass function. We further assume a constant SFR of 1 $M_{\odot}$ yr^{-1}, with an exponentially declining star formation history with timescales of $\tau_{\rm SFR} = 20$ Gyr. To convert these galaxy templates to colors, we first apply a dust extinction correction [34] with E(B-V) $= 0.0 - 0.4$. Second, we take into account the IGM absorption correction [35]. Then, we convolve the spectral energy distribution with the transmission curves of the five *HST* broad band filters to get the colors of the simulated galaxies. In the left panel of Extended Data Fig. 2, the dark blue dots are the low-redshift template galaxies with redshift from $z = 2.0 - 4.0$. The red points represent star-forming galaxies at $z = 5.5 - 6.5$. We use the following criteria to select galaxies at $z > 4$.

$$F606W - F814W > 2 \tag{1}$$

$$F814W - F105W < 3 \tag{2}$$

$$F606W - F814W > 1.5 \times (F814W - F105W) + 0.5 \tag{3}$$

Based on these criteria, we rule out almost all of the continuum sources as high redshift candidates, except for C1-1 and C5-3. In this panel, C1-1 and C5-3 are not detected in the F606W filter, which could indicate that they are V-dropout galaxy candidates. In the right panel of Extended Data

Fig. 2, we further study their color using the F814W, F105W and F125W filters, and the following criteria to select $z \approx 6$ galaxies:

$$F814W - F105W > 0.2 \tag{4}$$

$$F105W - F125W < 0.4 \tag{5}$$

$$F814W - F105W > 1.6 \times (F105W - F125W) + 0.36 \tag{6}$$

With these criteria, C1-1 is ruled out. However, C5-3 is located at the boundary of the above criteria. Therefore, except for C5-3, all the other targets are unlikely to be $z \approx 6$ candidates. We note that the broad band color has a weak redshift constraint ($\Delta z/(1+z) \sim 0.2$), so that even if C5-3 was a high redshift galaxy, it would have a small probability to be associated with the O I absorber. Since C5-3 was not detected in [C II] emission, its corresponding 3-σ [C II]-based SFR upper limit is $\mathrm{SFR}_{[\mathrm{CII}]} = 1\ M_\odot\ \mathrm{yr}^{-1}$. The ***HST*** observation and ALMA continuum emission indicate a UV- and TIR-based SFR of both $11\ M_\odot\ \mathrm{yr}^{-1}$, a factor of 10$\times$ higher than the 3-σ upper limit of the [C II]-based SFR. This further rules out that this source is located at $z = 5.978$.

Comparison between observations and different simulations. We compare the measured impact parameter and the derived halo mass of [C II]2054 and that of other three simulations, i.e., Sherwood, HVEL, and FAST simulations. These absorbers are selected with REWs of 0.12 ± 0.05Å. We find that, as the mass of host halo increases, absorbers can be ejected to increasing distances from the halo. These absorbers are located closest to the host halos with typical masses of $10^{10} M_\odot$. However, the derived halo mass of [CII]2054 is larger than one order of magnitude than the median value predicted by all of these simulations. Our results suggest that low-mass systems

in these simulations are overly efficient at producing metal absorbers.

28. McMullin, J. P., Waters, B., Schiebel, D., Young, W. & Golap, K. CASA Architecture and Applications. In Shaw, R. A., Hill, F. & Bell, D. J. (eds.) *Astronomical Data Analysis Software and Systems XVI*, vol. 376 of *Astronomical Society of the Pacific Conference Series*, 127 (2007).

29. Shapley, A. E., Steidel, C. C., Pettini, M. & Adelberger, K. L. Rest-Frame Ultraviolet Spectra of z~3 Lyman Break Galaxies. *APJ* **588**, 65–89 (2003). astro-ph/0301230.

30. Bertin, E. & Arnouts, S. SExtractor: Software for source extraction. *AAPS* **117**, 393–404 (1996).

31. Pavesi, R. *et al.* ALMA Reveals Weak [N II] Emission in "Typical" Galaxies and Intense Starbursts at z = 5-6. *APJ* **832**, 151 (2016). 1607.02520.

32. Ono, Y. *et al.* Great Optically Luminous Dropout Research Using Subaru HSC (GOLDRUSH). I. UV luminosity functions at z $\sim$ 4-7 derived with the half-million dropouts on the 100 deg^2 sky. *PASJ* **70**, S10 (2018). 1704.06004.

33. Bruzual, G. & Charlot, S. Stellar population synthesis at the resolution of 2003. *MNRAS* **344**, 1000–1028 (2003). astro-ph/0309134.

34. Calzetti, D. *et al.* The Dust Content and Opacity of Actively Star-forming Galaxies. *APJ* **533**, 682–695 (2000). astro-ph/9911459.

35. Inoue, A. K., Shimizu, I., Iwata, I. & Tanaka, M. An updated analytic model for attenuation by the intergalactic medium. *MNRAS* **442**, 1805–1820 (2014). 1402.0677.

Acknowledgements Z.C. and Y.W. are supported by the National Key R&D Program of China (grant No. 2018YFA0404503). M.N. acknowledges support from ERC Advanced grant 740246 (Cosmic_Gas). F.W. thanks the supports provided by NASA through the NASA Hubble Fellowship grant #HST-HF2-51448.001-A awarded by the Space Telescope Science Institute, which is operated by the Association of Universities for Research in Astronomy, Incorporated, under NASA contract NAS5-26555.

Author contributions All authors discussed the results and commented on the manuscript. Y.W. and Z.C. led the data reduction, pipeline development, analysis and manuscript writing. Z.C., M.N., K.F., N.K. and J.X.P. conceived the project and led the telescope proposal. M.N., K.F., N.K. and S.Z. all participated the analysis and data reduction. R.W. helped checking of the ALMA data reduction and analysis. X.F., L.K., F.W., J.Y., J.H. and J.W. all have significant helps on the interpretation and commented on the ALMA proposal and the paper.

Data Availability Both ALMA and HST data used in this work have been public available. The data reported in this paper are available though the ALMA archive: (http://almascience.eso.org/aq/) with project code: 2017.1.01088.S, the HST (https://archive.stsci.edu/hst/) with project code: 15410 and 12974.

Code Availability The ALMA data were reduced using the CASA pipeline version 5.4.0, available at https://casa.nrao.edu/casa_obtaining.shtml.

Competing interests The authors declare no competing interests.

Correspondence Correspondence and requests for materials should be addressed to Z.C. and Y.W. (email: zcai@mail.tsinghua.edu.cn, yj-wu19@mails.tsinghua.edu.cn)

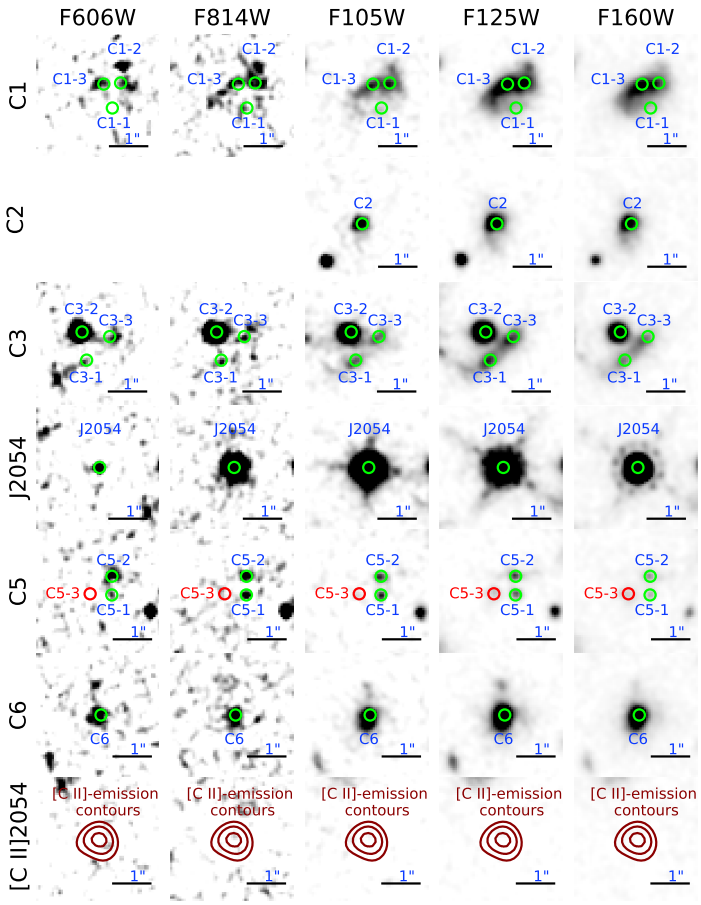

Extended Data Fig. 1. High-resolution *HST* broad-band images for five different filters. These images are sorted by the filter central wavelength. From left to right, these images are F606W, F814W, F105W, F125W, and F160W, respectively. The *HST* photometry is based on apertures with a 0.3 arcsec diameter, as shown by the green and red circles. The darkred contours (2-4σ) represent the [C II]-emission region in the ALMA [C II] narrow band image. We find no continuum emission in this region in all five *HST* images.

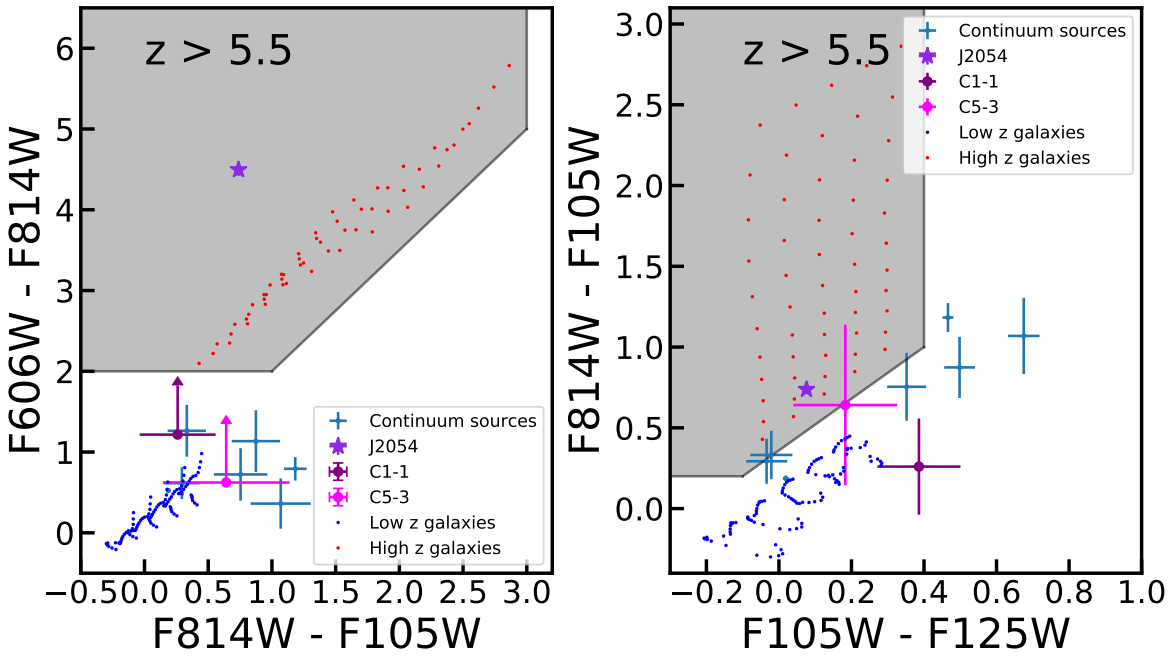

Extended Data Fig. 2. Color-color diagrams used to select galaxies associated with the O I absorber. The continuum sources are plotted in blue circles. The red and dark blue dots represent the color properties of simulated star-forming galaxies at $z > 5.5$ and $z < 4$, respectively. Our star-forming templates are the same as [32]. High-redshift selection criteria are based on the distribution of these template galaxies. *Left:* $I - Y$ vs. $V - I$ two color diagram. In the left panel, we rule out most continuum sources as high-redshift galaxies, except for C1-1 and C5-3. These two galaxies have the same color properties as the simulated high redshift galaxies, and are plotted as a purple and magenta dot. *Right:* $Y - J$ vs. $I - Y$ two color diagram. In the right panel, we rule out C1-1 as a high-redshift candidate. However, C5-3 is still consistent with the other simulated high-redshift galaxies. QSO J2054-0005 is plotted as a blue-violet star.

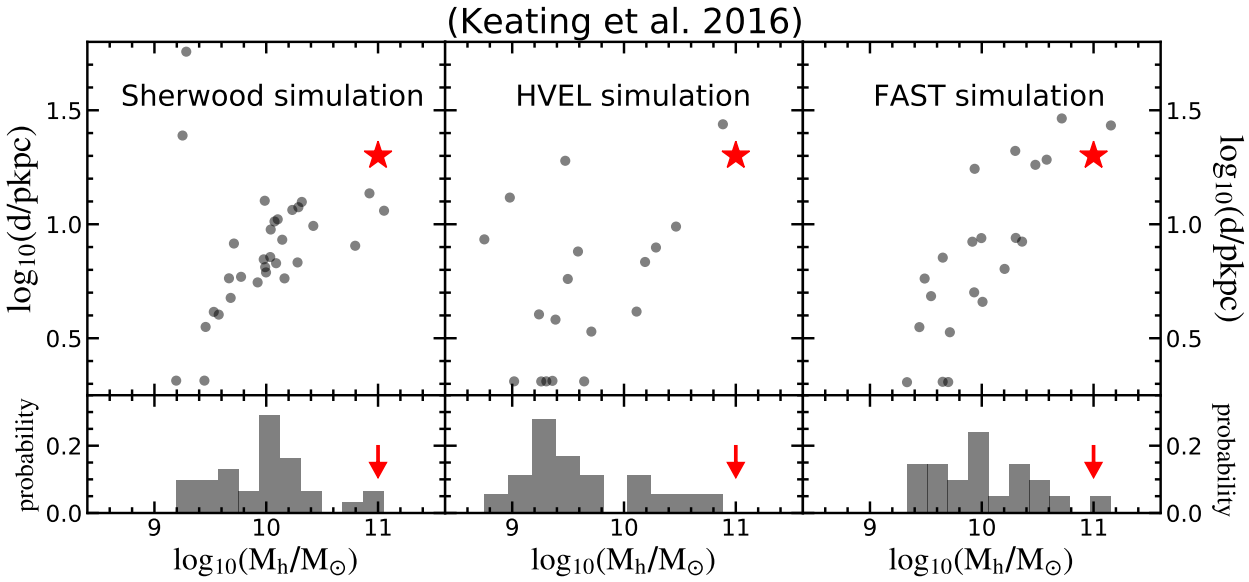

Extended Data Fig. 3. .The relationship between the projected impact parameters and halo masses of strong O I absorbers in different simulations[16]. In the three top panels, grey dots represent O I absorbers with the REW of 0.12 ± 0.05 Å (consistent with observations). Meanwhile, Red star represents [C II]2054. In the bottom panels, Red arrow shows that the host halo mass of [C II]2054 is larger than one order of magnitude than the median value predicted by all of these simulations. Our observations strongly constrain all of these simulations.

Figures

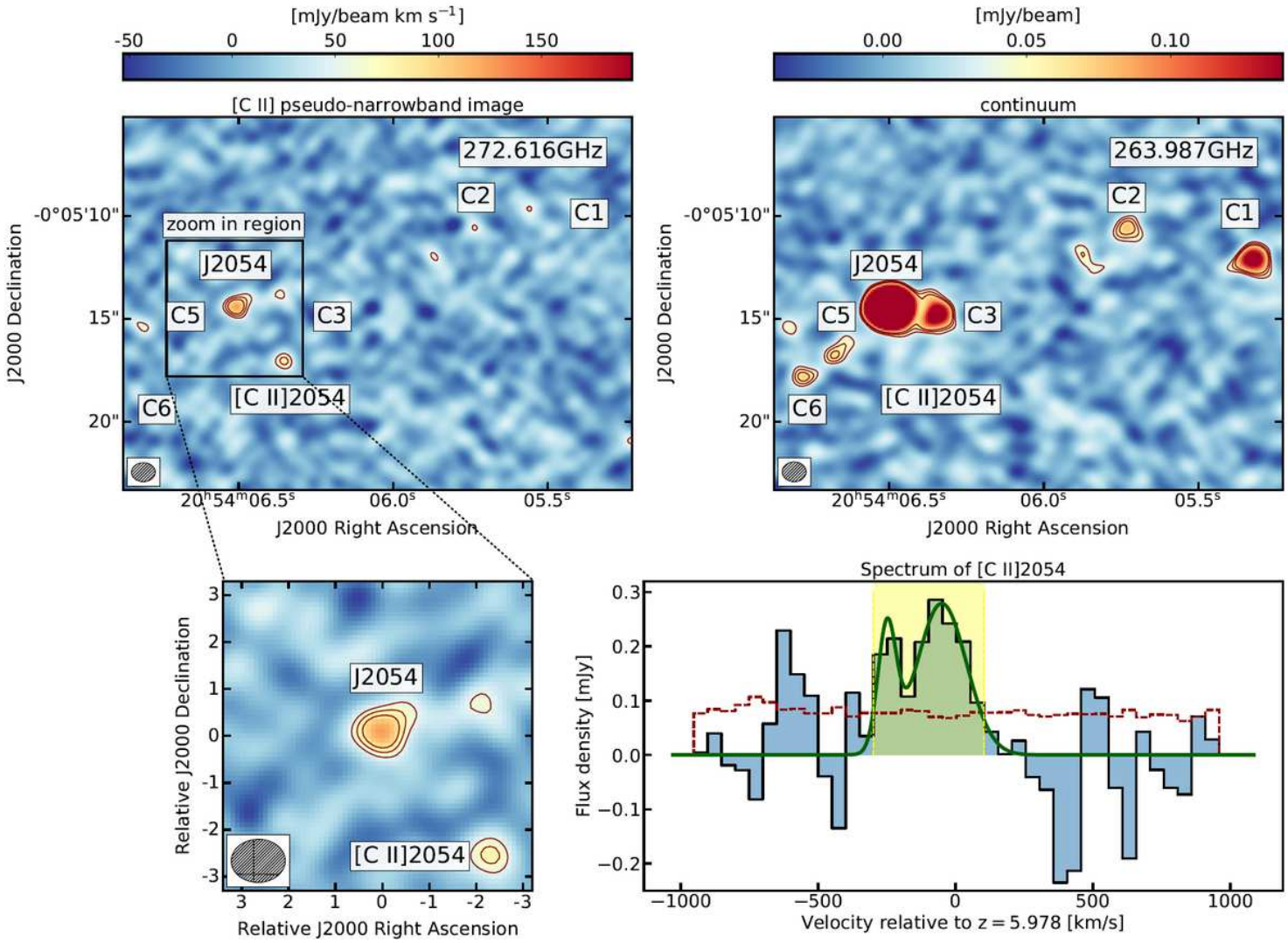

Figure 1

ALMA observations. a, Integrated [C II] pseudo-narrowband image. The outer contour is at 3σ level, with contours in steps of 1-σ. The 1-σ is 1.76 × 10−2Jy beam−1 km s−1, calculated using the pixel-to-pixel standard deviation. The QSO is detected in the continuum-subtracted image because of a water line at this frequency. b, 263.987 GHz continuum map. Contours are drawn at [3, 4, 5]×σ. In this map, the 1-σ noise is 12.6 μJy beam−1. Six continuum sources within 2000 can be seen. C4 is the QSO J2054. c, Zoom-in [C II] pseudo-narrow band image. The sizes of the synthesized beams are plotted in the bottom-left of these panel. d, Spectrum of [C II]2054. The darked dashed line shows the 1-σ rms noise. The narrow-band [C II] image is collapsed based on the emission range shown by the yellow-shaded region. The velocity is relative to the O I redshift z = 5.978. The darkgreen line shows a double Gaussian model fit to the data. The integral [C II] flux is 0.078 ± 0.013 Jy km s−1.

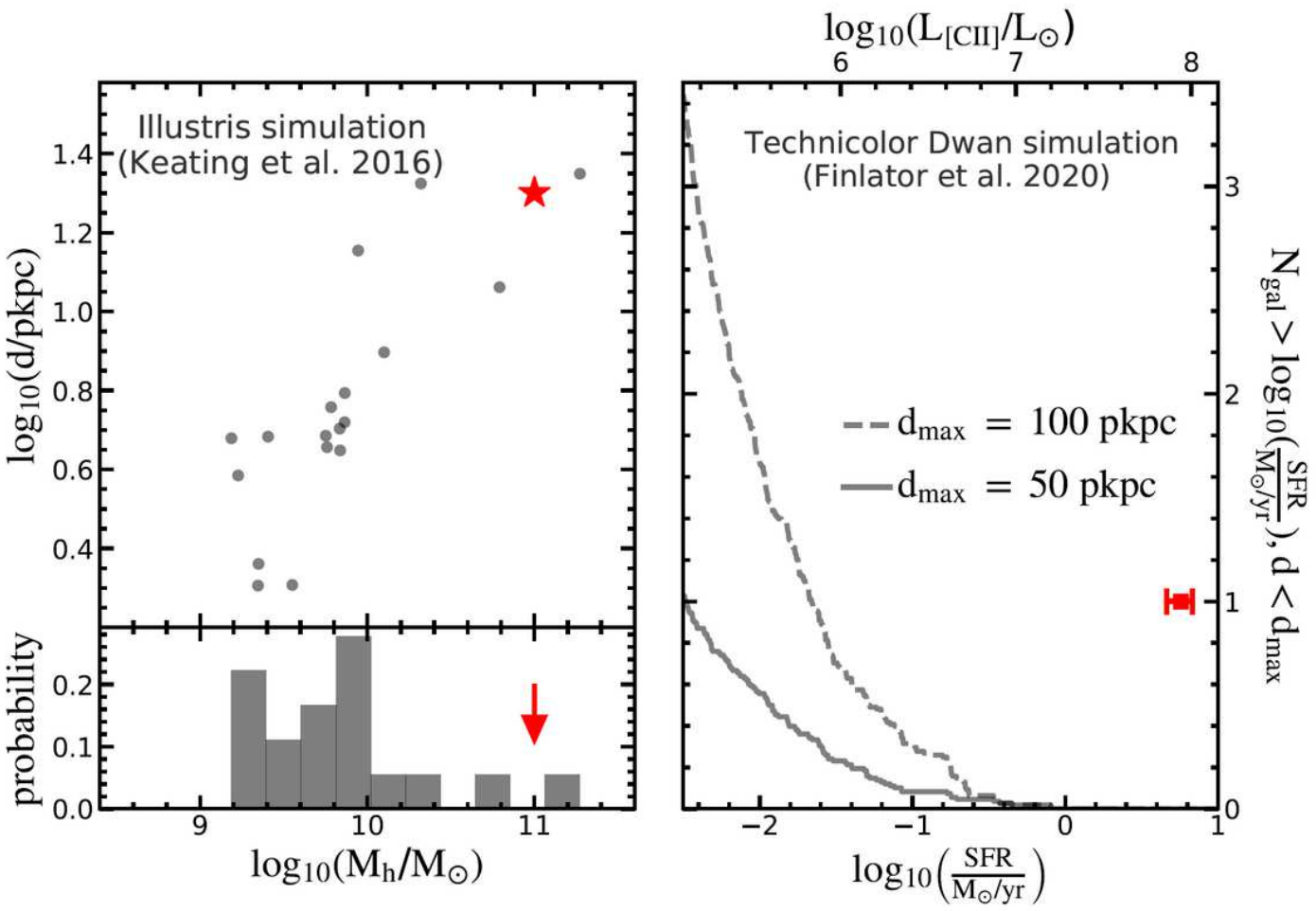

Figure 2

Comparison between simulations and observations. Left Upper: The relationship be tween projected impact parameter and halo mass of strong O I absorbers in the Illustris simulation16. The O I absorbers have the rest-frame equivalent width of 0.12 ± 0.05 Å (consistent with observations). Red star represents [C II]2054. Left Bottom: Red arrow shows that the host halo mass of [C II]2054 is larger than one order of magnitude than the median value predicted by Illustris simulations. Right: The number of galaxies that cluster about strong O I absorbers at z = 6 is predicted to vary with SFR (y-axis is arbitrary). The solid and dashed curves are biased star formation rate functions 10. They are generated by accumulating catalogs of all galaxies that fall within 50 or 100 pkpc of O I absorbers with REW > 0.12Å (NO I > 1014.2cm−2). The predicted luminosity of O I associated [C II] emitter is roughly two orders of magnitude fainter than [C II]2054.

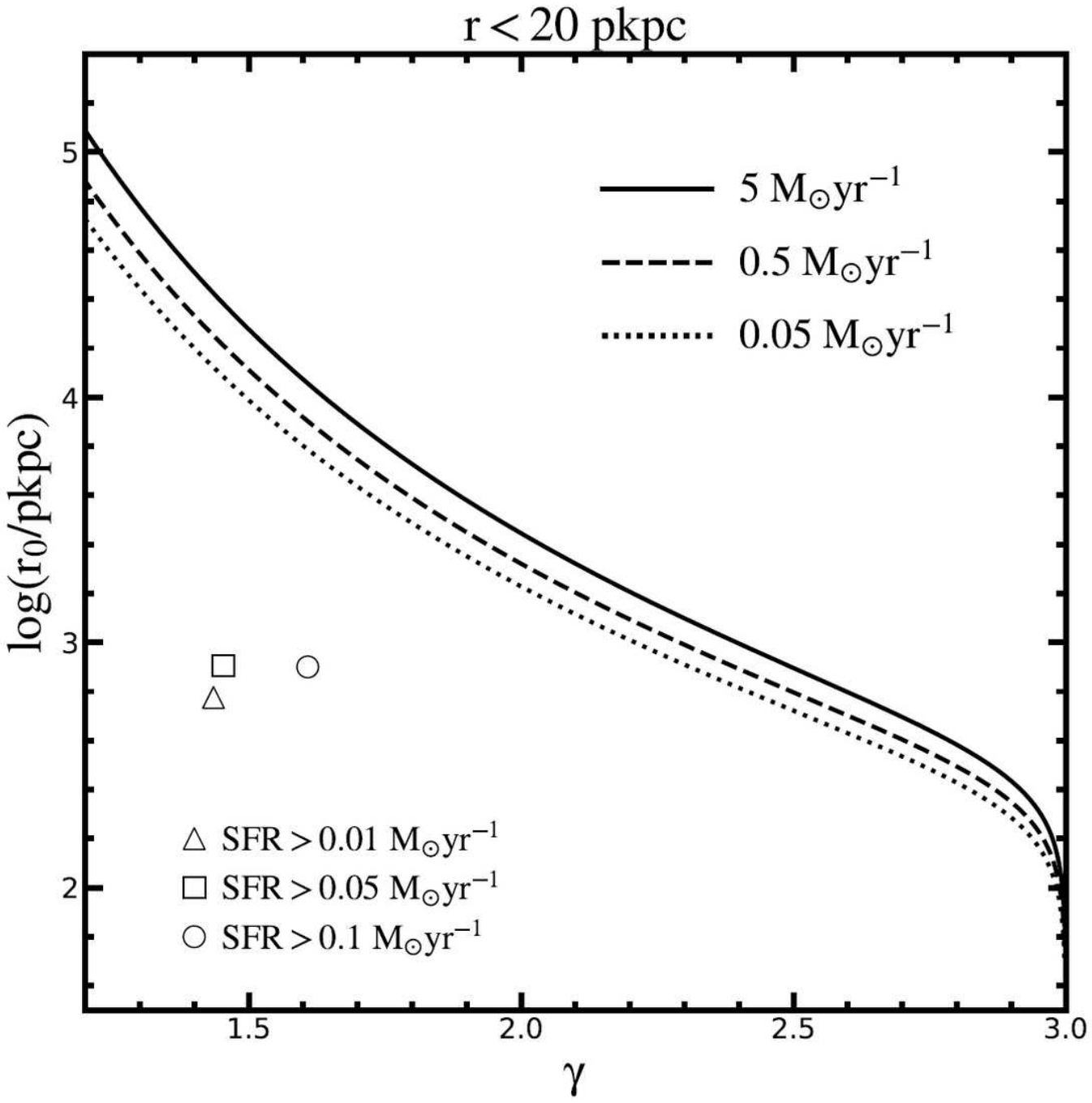

Figure 3

Comparison of cross-correlation function between simulations and observations. We assume the galaxy-absorber cross-correlation as ξ(r) = (r/r0)−γ. This function expresses the fractional excess number density of galaxies located at a distance r from an absorber in terms of the correlation length r0 and a power-law slope γ. Shaped points indicate cross-correlation functions predicted by Technicolor Dawn for galaxies clustered about synthetic OI absorbers with REW ≥ 0.12Å. The solid, dashed and dotted line shows that predict an average of one galaxy of SFR ≥ 5, 0.5 and 0.05 M /yr, within 20.0 pkpc of an absorber at z =

5.9, respectively. Comparing with shaped dots, the predicted r0 is 10× too low to explain the observations.

Supplementary Files

This is a list of supplementary files associated with this preprint. Click to download.

- table.pdf
- figure4.pdf
- figure5.pdf
- figure6.pdf